Renewable Microgrid Protection Strategy Coordinating with Current-based Fault Control

Zihao Wang, Longhua Mu, and Chongkai Fang

***Abstract*—The renewable microgrid (RMG) is a critical way to organize and utilize new energy. Its control and protection strategies during the fault are the core technologies to ensure the safe operation and stability of the system. The traditional protection principles are unsuitable for RMGs due to the flexibility of RMG operation, the complexity of RMG topology, and the variety of fault control strategies of inverter-interfaced distributed generators (IIDGs). The traditional fault component protection principle is affected by the low voltage ride-through (LVRT) control strategy and will fail in some scenarios. In order to make the fault component protection principle available in every scenario, a current-based fault control strategy is proposed. Specific fault characteristics are generated by the grid-feeding IIDGs during the fault so they can be equivalent to the open circuits, and the fault models in additional network can be simplified. By analyzing the fault characteristics, an RMG protection strategy based on the current-based fault control of IIDGs is presented. The fault directions of feeders can be distinguished and the fault feeder can be located accurately in both grid-connected and islanded RMGs. Then, the grid-feeding IIDGs can transit to LVRT mode smoothly. Thus, IIDGs are considered comprehensively in terms of coordinating with fault control and fault characteristic generation. Finally, the experimental results of the hardware platform prove the effectiveness of the proposed current-based fault control strategy, and the simulation results based on PSCAD/EMTDC verify the correctness of the protection strategy.**

***Index Terms*—Renewable microgrid, protection strategy, fault characteristic, control strategy, fault component.**

I. Introduction

DUE to the primary energy depletion and increasing environmental pressures, renewable energy sources (RESs) are growing rapidly around the world [1], [2]. Many countries emphasize the use of RESs such as solar and wind to achieve energy efficiency improvement and carbon emission reduction. In order to integrate distributed renewable energy into the power system, the renewable microgrid (RMG) can be regarded as an effective and feasible solution. RMGs are electricity distribution systems containing loads and distributed generations (DGs), which can promote mass access of DG and renewable energy [3], [4].

The penetration of RESs in distribution system has led to the rapid development of RMGs and brought new challenges. Control systems of RMGs must be responsive to fluctuations and randomness of RESs. It is necessary to adjust the control strategy to recover the RMG from the effects of abnormalities and faults. DGs are connected to the RMG through inverters, which realizes the function of plug-and-play and the local consumption of new energy [5]. There are many control strategies for DGs, which are the cores of determining their output and fault characteristics [6]. Due to RMG operation modes and topologies and fault characteristics of inverter-interfaced distributed generators (IIDGs), the conventional protection principles are no longer applicable and are unable to locate the fault feeders from RMGs quickly and selectively. Therefore, the control and protection coordination strategy is the state-of-the-art technology to generate specific fault characteristics, which realizes the coordination design of fault control and protection strategy.

The IIDG system, as shown in Fig. 1, is mainly composed of prime mover and grid-side converter (GSC). It is widely used in the photovoltaic (PV), battery, and type-4 wind turbine generator.

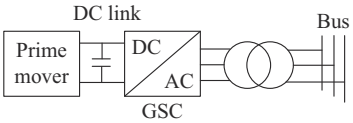

Fig. 1. Simplified model of IIDG system.

Opposed to the traditional power systems, RMGs comprised of IIDGs cannot provide large fault power and current like synchronous generators due to the limitation of semiconductors [7]-[9]. The intermittence of IIDGs leads to the variable amplitudes and directions of the fault power. Such variations result in the limitations of the application of traditional protection methods in RMGs [10]-[12]. An optimization technique of time multiplying setting (TMS) was proposed in [13] to improve the limitations in the tripping characteristics of overcurrent relays. However, the changeable topologies of RMGs will lead to different overcurrent characteristics so that the TMS should be changed on-time to satisfy the plug-and-play function of IIDGs. When the operation mode or topology of RMGs changes, the adaptive protection scheme

Manuscript received: February 11, 2022; revised: May 17, 2022; accepted: July 5, 2022. Date of CrossCheck: July 5, 2022. Date of online publication: July 22, 2022.

This work was supported by the Fundamental Research Funds for the Central Universities (No. 22120210164).

Z. Wang, L. Mu (corresponding author), and C. Fang are with the College of Electronics and Information Engineering, Tongji University, Shanghai 201804, China (e-mail: zhwang@tongji. edu. cn; lhmu@tongji. edu. cn; 2011248@tongji. edu.cn).

DOI: 10.35833/MPCE.2022.000079

will automatically modify the threshold values of relays [14]-[16]. However, it needs a central protection unit to monitor the operation mode of RMGs.

In addition to ameliorating the traditional overcurrent protections to adapt to RMGs, some scholars also pay attention to some new protection schemes based on intelligent algorithm or communication. An intelligent method for fault detection by using the undecimated wavelet transform is proposed in [17]. Only the voltage quantities are required to monitor the power quality disturbance of a PV microgrid. However, due to the large number of PVs, the complex topology of microgrids, and the calculation difficulty of short-circuit faults, the computation burden of adaptive tuning is huge. Therefore, it poses a challenge for the central controller to ensure the real-time protection. A new impedance-matrix-based method is proposed in [18], which uses the pre-fault and during-fault voltage phasors at few buses to locate the fault feeder. However, in case of high impedance faults, its detection accuracy will decrease. Besides, differential protection schemes are suggested in [19]-[21], but communication units are needed at both ends of the feeder.

The fault control strategy for IIDGs has a decisive impact on the fault characteristics [22]-[24]. Due to the small inertia and fast response of IIDGs [25]-[27], some scholars begin to focus on RMG protection schemes which adjust the IIDG control strategy when a fault occurs in the RMG [28], [29]. Reference [30] proposes a protection scheme in which the IIDG injects the fifth harmonic into the short-circuit current under RMG fault conditions. By detecting the ratio of the fifth harmonic in fault currents, the fault feeder can be located. However, this scheme is only verified in a simple low-voltage microgrid. In a complex medium-voltage RMG, the thresholds of ratios and the protection reliability may be affected by the nonlinear loads and the network topology. In [31], by measuring the equivalent impedance of point of common coupling (PCC), IIDGs in a ring RMG are controlled to output current in equal proportion so that the traditional overcurrent protection could be applied. However, measuring the PCC equivalent impedance is not an easy task, and this scheme is only effective for specific RMG structures. A new impedance-based fault detection method is proposed in [32], which considers multiple types of DGs and faults. However, this method relies highly on positive- and negative-sequence electrical quantities to distinguish the symmetrical and asymmetrical faults.

In this paper, a current-based fault control strategy of grid-feeding IIDGs and an RMG protection strategy are proposed. The output currents of grid-feeding IIDGs are maintained to simplify the positive-sequence additional network of the RMG. By analyzing the fault characteristics of the RMG, the phase difference between the positive-sequence current fault component (PSCFC) and the pre-fault bus voltage is used to distinguish the fault direction of the feeder, and the fault feeder can be located accurately in both grid-connected and islanded modes. Finally, the effectiveness of the proposed RMG protection strategy is verified by PSCAD/EMTDC. This strategy only needs modification to the control strategy of IIDGs without adding expensive hardware devices in the RMG.

The rest of this paper is structured as follows. The fault component protection principle and its limitation are presented in Section II. The current-based fault control strategy adapting to the fault component protection principle is explained in Section III. Section IV presents a new RMG protection strategy based on the current-based fault control strategy of IIDGs. Experimental results are presented in Section V. Discussion and comparison of the proposed control and protection strategy to other strategies are presented in Section VI. Section VII concludes the paper.

II. Fault Component Protection Principle and Its Limitation

A. Fault Component Principle

Based on the superposition principle, a current or voltage variable can be regarded as two components: a normal-running component and a fault component. The fault component can be calculated using superimposed networks [33]. Assuming that $i_{\mathrm{n}}(t)$ and $v_{\mathrm{n}}(t)$ are the current and voltage of the normal-running system, respectively, $i_{\mathrm{f}}(t)$ and $v_{\mathrm{f}}(t)$ are the current and voltage of the faulty system, respectively, the fault components of current and voltage $\Delta i_{\mathrm{f}}(t)$ and $\Delta v_{\mathrm{f}}(t)$ can be expressed as:

$$\begin{cases} \Delta i_{\mathrm{f}}(t) = i_{\mathrm{f}}(t) - i_{\mathrm{n}}(t) \\ \Delta v_{\mathrm{f}}(t) = v_{\mathrm{f}}(t) - v_{\mathrm{n}}(t) \end{cases} \tag{1}$$

As (1) indicates, the fault component of current or voltage can be calculated by subtracting the normal-running (pre-fault) current or voltage from the fault (during-fault) current or voltage.

In discrete-time mode, (1) can be expressed as:

$$\begin{cases} \Delta i_{\mathrm{f}}(k) = i_{\mathrm{f}}(k) - i_{\mathrm{n}}(k-N) \\ \Delta v_{\mathrm{f}}(k) = v_{\mathrm{f}}(k) - v_{\mathrm{n}}(k-N) \end{cases} \tag{2}$$

where k is the sampling time; and N is the number of sampling points per period.

Equation (2) indicates that the fault component is the difference of electrical quantity between cycles. Thus, the fault components do not exist under normal conditions but appear if a fault occurs in the RMG.

B. Low Voltage Ride-through (LVRT) Code of IIDGs

Under normal conditions, IIDGs only output positive-sequence power to RMGs. According to the instantaneous power theory, in the synchronous rotating reference frame, the average value of active power output P_{out} and reactive power output Q_{out} of IIDGs can be expressed as:

$$\begin{cases} P_{\mathrm{out}} = \dfrac{3}{2} U_d^+ I_{d,\mathrm{ref}} \\ Q_{\mathrm{out}} = -\dfrac{3}{2} U_d^+ I_{q,\mathrm{ref}} \end{cases} \tag{3}$$

where U_d^+ is the d-axis component of the positive-sequence PC voltage; and $I_{d,\mathrm{ref}}$ and $I_{q,\mathrm{ref}}$ are the d-axis and q-axis components of current reference signal, respectively.

In terms of the German grid code, IIDGs need to output positive-sequence current and reactive power to support the

RMG under fault conditions [8]. The current can be expressed as:

$$I_q = \begin{cases} 0 & 0.9 < U_d^+ \le U_{\mathrm{n}} \\ 2I_{\max}\left(1 - \dfrac{U_d^+}{U_{\mathrm{n}}}\right) & 0.5 < U_d^+ \le 0.9U_{\mathrm{n}} \\ I_{\max} & 0 < U_d^+ \le 0.5U_{\mathrm{n}} \end{cases} \tag{4}$$

where I_q is the reactive fault current; U_{n} is the normal-running voltage; and $I_{\max}$ is the maximum output current of IIDGs.

Combining (3) and (4), it can be concluded that the IIDG connected to an RMG can be equivalent to a current source controlled by U_d^+.

C. Application of Fault Component Protection Principle

According to the IEEE 1547 standard, an RMG model is shown in Fig. 2, which contains battery energy storage system (BESS), wind turbine (WT), and PV. LD1, LD2, and LD3 are loads; DG1, DG2, DG3, and DG4 are IIDGs; A1-A4, B1-B4, C1-C3, and D1-D3 are the circuit breakers (CBs) of feeders. The RMG is connected to the utility grid through a PCC switch.

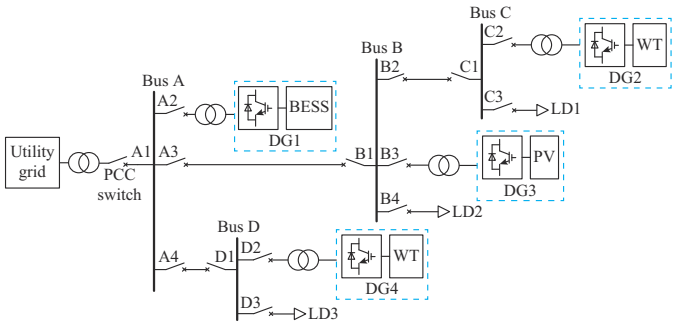

Fig. 2. RMG model.

DG2-DG4 represent the grid-feeding IIDGs like PVs or type-4 WTs, which adopt the LVRT codes and thus can be equivalent to current sources. DG1 represents a grid-forming IIDG like BESS or fuel cell, which can be used as the main power source in the islanded RMG to provide stable voltage and frequency for the bus. Thus, in the islanded mode, DG1 can be equivalent to a voltage source. However, in the grid-connected mode, DG1 should also adopt the LVRT code and thus can be equivalent to a current source.

Positive-sequence fault components exist under all types of RMG fault conditions [34]. When a fault occurs at point *F*, the equivalent additional network of the positive-sequence fault component is shown in Fig. 3.

In Fig. 3, $\Delta \boldsymbol{u}_{\mathrm{f}}$ is the additional positive-sequence voltage source at the fault point *F*; $\Delta \boldsymbol{i}_{\mathrm{DG1,f}}$, $\Delta \boldsymbol{i}_{\mathrm{DG2,f}}$, $\Delta \boldsymbol{i}_{\mathrm{DG3,f}}$, and $\Delta \boldsymbol{i}_{\mathrm{DG4,f}}$ are the equivalent additional positive-sequence currents of DG1, DG2, DG3, and DG4, respectively; Z_x is the equivalent positive-sequence impedance, whose subscript x indicates the name of feeders or loads; and $\Delta \boldsymbol{i}_{\mathrm{A1}}$ - $\Delta \boldsymbol{i}_{\mathrm{A4}}$, $\Delta \boldsymbol{i}_{\mathrm{B1}}$ - $\Delta \boldsymbol{i}_{\mathrm{B4}}$, $\Delta \boldsymbol{i}_{\mathrm{C1}}$ - $\Delta \boldsymbol{i}_{\mathrm{C3}}$, and $\Delta \boldsymbol{i}_{\mathrm{D1}}$ - $\Delta \boldsymbol{i}_{\mathrm{D3}}$ are the PSCFCs at Buses A-D, respectively. In Fig. 3(a), DG1 operates as a master power source and can be equivalent to an impedance in the islanded mode. In Fig. 3(b), DG1 adopts the LVRT code and thus can be equivalent to an additional positive-sequence voltage controlled current source.

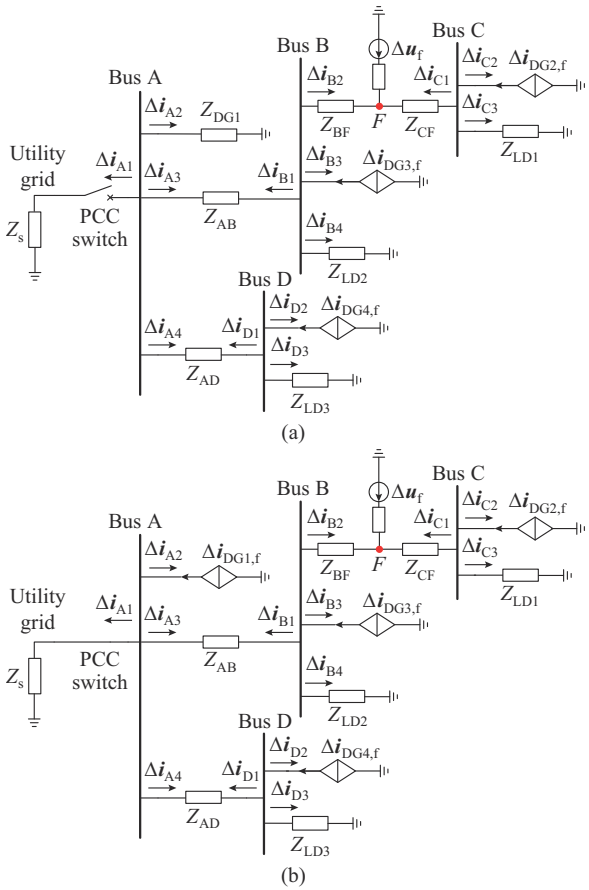

Fig. 3. Equivalent additional network of positive-sequence fault component when a fault occurs at point *F*. (a) Islanded mode. (b) Grid-connected mode.

D. Limitation of Fault Component Protection Principle

It is assumed that the positive direction of current is from bus to feeder, as shown in Fig. 3. If the current direction of a feeder is consistent with the fault direction, it is defined as a forward fault feeder. Otherwise, it is a reverse fault feeder. For example, in case of a fault at *F*, the feeders of A3, B2, C1, and D1 are forward fault feeders.

According to the LVRT code, the grid-feeding IIDGs can be equivalent to voltage controlled current sources in LVRT mode. Taking DG3 as an example, the change of output current is shown in Fig. 4(a). $\boldsymbol{u}_{\mathrm{B,0}}$ and $\boldsymbol{u}_{\mathrm{B,f}}$ are the pre-fault and during-fault voltages of Bus B, respectively; $\boldsymbol{i}_{\mathrm{DG,0}}$ and $\boldsymbol{i}_{\mathrm{DG,f}}$ are the pre-fault and during-fault output currents of DG3, respectively; $\Delta \boldsymbol{i}_{\mathrm{DG,f}}$ is the fault component of output current of DG3; and θ is the angle between the output fault current $\boldsymbol{i}_{\mathrm{DG,f}}$ and $\boldsymbol{u}_{\mathrm{B,f}}$. According to the LVRT code in (4), as the reactive power output of IIDG increases, θ increases within the sector region enclosed by an arc with the radius of I_{lim}. The fault component $\Delta \boldsymbol{i}_{\mathrm{DG,f}}$ changes within the light gray region in Fig. 4(a). According to the change of output current of IIDG in Fig. 4(a), the phasors of PSCFC are shown in Fig. 4(b).

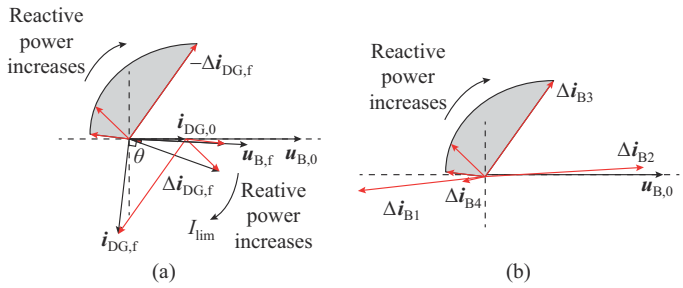

Fig. 4. Output current of IIDG and phasors of PSCFC at Bus B. (a) Output current of IIDG. (b) Phasors of PSCFC.

Take the change range of PSCFC of feeder B3 as an example. With the increases of output reactive power of IIDG, the phase difference between fault component $\Delta \boldsymbol{i}_{B3}$ and pre-fault bus voltage $\boldsymbol{u}_{B,0}$ will change from 90°-180° to 0°-90°. At this time, the fault feeder cannot be located by the phase relationship between the PSCFC and the pre-fault bus voltage. Therefore, the fault component protection principle based on phase comparison cannot be applicable in some situations.

The traditional fault component protection principle is limited by the operation mode and the topology of RMGs, and the LVRT control strategy of IIDGs will also affect fault characteristics of RMGs.

III. Current-based Fault Control Strategy Adapting to Fault Component Protection Principle

A. Proposed Current-based Fault Control Strategy

The control strategy of IIDGs in an RMG affects the fault characteristics and the positive-sequence additional network model of the RMG, which leads to the failure of the fault component protection principle. According to the analysis in Section II, the grid-feeding IIDGs can be equivalent to current sources in the positive-sequence fault component network. By adjusting the current control strategy of grid-feeding IIDGs, the fault models can be simplified and the fault component protection principle can still be applicable. A proposed current-based control strategy of IIDG is shown in Fig. 5.

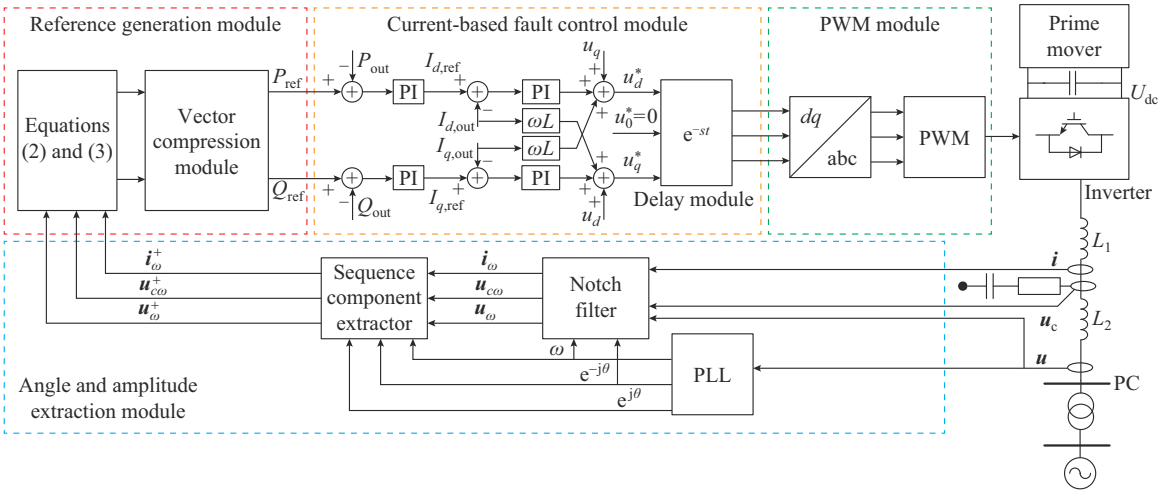

Fig. 5. Proposed current-based fault control strategy of IIDG.

In Fig. 5, the PLL stands for phase locked loop; PWM stands for pulse width modulation; PI stands for proportional-integral controller; PC stands for point of coupling; the notch filter is used to extract the positive-sequence electrical quantities; P_{ref} and Q_{ref} are the reference values of active and reactive power, respectively; $I_{d,out}$ and $I_{q,out}$ are the d-axis and q-axis components of the output current, respectively; u_d and u_q are the d-axis and q-axis components of the output voltage, respectively; and u_d^*, u_q^*, and u_0^* are the reference values of the d-axis, q-axis, 0-axis components of the voltage, respectively; $\boldsymbol{i}_\omega$ is the output current; $\boldsymbol{u}_{c\omega}$ is the capacitor voltage; $\boldsymbol{u}_\omega$ is the voltage of RMG; and the superscript + represents the positive-sequence electrical quantities.

In the angle and amplitude extraction module, a notch filter and a sequence component extractor are combined to extract the positive-sequence electrical quantities $\boldsymbol{i}_\omega^+$, $\boldsymbol{u}_{c\omega}^+$, and $\boldsymbol{u}_\omega^+$. In the reference generation module, a vector compression module is used to limit the reference value of the output current and power in equal proportion to ensure that the IIDG works in a safe range. Based on the current-based fault control module, with a delay module, the output current of IIDG can be maintained for a period of time. Considering the state-of-the-art power electronics control technology and the fault transient process, the delay time is 2 cycle in this paper. Thus, the PSCFCs of the grid-feeding IIDGs in (1) can be expressed as:

$$0 = i_f^+(t) - i_n^+(t) \tag{5}$$

where $i_f^+(t)$ and $i_n^+(t)$ are the positive-sequence current under fault and normal conditions, respectively.

B. Analysis of RMG Fault Characteristics Based on Proposed Current-based Fault Control Strategy

Owing to the proposed current-based fault control strategy, the PSCFCs of IIDGs are zero during the fault. Therefore, the fault models shown in Fig. 3 can be simplified. Since the fault components of output currents of grid-feed-

ing IIDGs are 0, the grid-feeding IIDGs can be equivalent to open circuits. The additional network of the positive-sequence fault component based on proposed current-based fault control strategy is shown in Fig. 6.

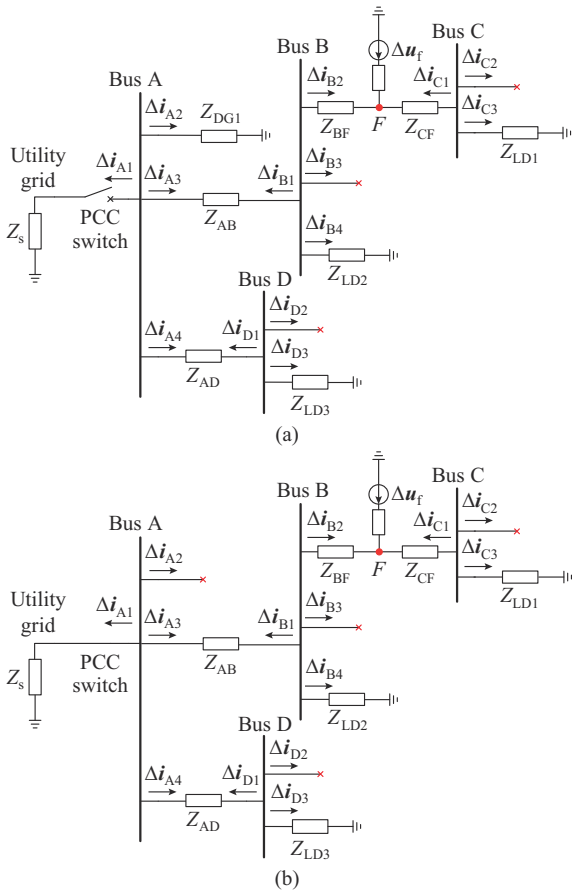

Fig. 6. Additional network of positive-sequence fault component based on proposed current-based fault control strategy. (a) Islanded mode. (b) Grid-connected mode.

The PSCFC of the forward fault feeder at Bus K (K=A, B, C, D) can be expressed as:

$$\Delta \boldsymbol{i}_{\mathrm{K}i} = \sum_{j \neq i, j=1}^{n} \Delta \boldsymbol{i}_{\mathrm{K}j} \tag{6}$$

where $\Delta \boldsymbol{i}_{\mathrm{K}i}$ is the PSCFC of the forward fault feeder; $\Delta \boldsymbol{i}_{\mathrm{K}j}$ is the PSCFC of the reverse fault feeder; and n is the number of branch feeders contained at Bus K.

The PSCFC of the reverse fault feeder at Bus K can be expressed as:

$$\Delta \boldsymbol{i}_{\mathrm{K}j} = -\frac{Z'_{\mathrm{eq}}}{Z_{\mathrm{eq}} + Z'_{\mathrm{eq}}} \Delta \boldsymbol{i}_{\mathrm{K}i} \tag{7}$$

where Z'_{eq} is the equivalent positive-sequence impedance at the forward fault feeder side; and Z_{eq} is the equivalent positive-sequence impedance at the other feeder side. Z'_{eq} and Z_{eq} are mainly composed of positive-sequence impedances of feeders and loads, which means the impedance angles of Z'_{eq} and Z_{eq} are nearly equal. Therefore, it can be observed from (7) that the phasors of PSCFC of forward fault feeders and reverse fault feeders are different, and the corresponding phasors are shown in Fig. 7, where $\boldsymbol{u}_{\mathrm{K}}$ is the pre-fault bus voltage.

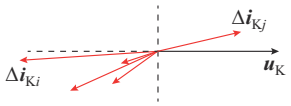

Fig. 7. Phasors of PSCFC at Bus K.

Based on the above analysis, it can be concluded that the feeders on the same bus have the following fault characteristics.

1) The equivalent impedances in (7) will only affect the amplitude of currents, but not the direction.

2) The phasor of PSCFC of forward fault feeders is almost opposite to that of reverse fault feeders.

3) The phase difference between the PSCFC of forward fault feeders and $\boldsymbol{u}_{\mathrm{K}}$ is less than 90°; the phase difference between the PSCFC of reverse fault feeders and $\boldsymbol{u}_{\mathrm{K}}$ is around 90°-180°.

4) Owing to the proposed current-based fault control strategy of IIDGs, the phase relationship in 3) is independent of the topology, parameters, and operation modes of RMGs.

IV. RMG Protection Strategy Based on Current-based Fault Control of IIDGs

A. Fault Starting Criterion

Considering the small short-circuit current provided by IIDGs during RMG fault, the change of positive-sequence voltage of fault feeder is not obvious under high-impedance faults. Therefore, the amplitudes of the bus voltage fault components are selected as the starting criterion:

$$\left|\Delta \boldsymbol{u}^{+}\right| + \left|\Delta \boldsymbol{u}^{-}\right| + \left|\Delta \boldsymbol{u}^{0}\right| > U_{\mathrm{set}} \tag{8}$$

where $\Delta \boldsymbol{u}^{+}$, $\Delta \boldsymbol{u}^{-}$, and $\Delta \boldsymbol{u}^{0}$ are the positive-, negative-, and zero-sequence voltage fault components of a bus, respectively; and U_{set} is the starting threshold. In this study, U_{set} is assumed to be 0.02 times the rated voltage U_{rate}.

B. Fault Detection Criterion

According to the analysis in Section II, the fault feeder can be recognized by fault characteristics, because the amplitude is affected by the RMG operation modes and the types of faults. If two feeders have a similar amplitude of voltage, the fault feeder cannot be distinguished reliably. Hence, the phase difference between the PSCFC of the feeder and the pre-fault bus voltage can be selected as the fault characteristic and used to detect the fault feeder.

According to the analysis results of fault characteristics, the fault detection criterion for the forward fault feeder can be described as:

$$0° < \left|\arg(\boldsymbol{u}_{\mathrm{K}}) - \arg(\Delta \boldsymbol{i}_{\mathrm{K}i})\right| < 90° \tag{9}$$

For the reverse fault feeders, the fault detection criterion can be described as:

$$90° < \left|\arg(\boldsymbol{u}_{\mathrm{K}}) - \arg(\Delta \boldsymbol{i}_{\mathrm{K}j})\right| < 180° \tag{10}$$

C. Proposed RMG Protection Strategy

By employing the proposed fault starting criterion and fault detection criterion, the fault direction of each feeder can be determined by (9) and (10). Based on the proposed current-based fault control strategy and fault detection criteria, the flow chart of the proposed RMG protection strategy under fault conditions is depicted in Fig. 8.

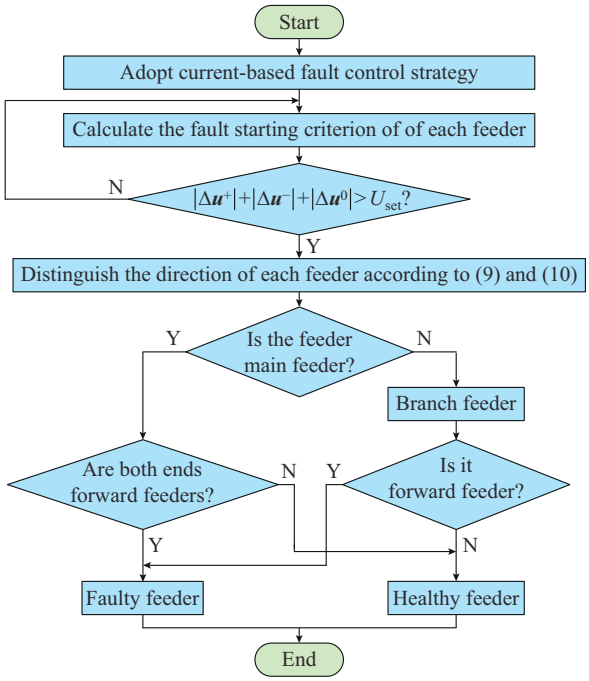

Fig. 8. Flow chart of proposed RMG protection strategy under fault conditions.

V. Experimental Results

In order to verify the effectiveness of the proposed current-based fault control strategy shown in Fig. 5, the simplified model of IIDG utilized in the hardware platform and PSCAD/EMTDC is presented in Fig. 9. A conventional two-level three-leg three-phase inverter is applied in this paper.

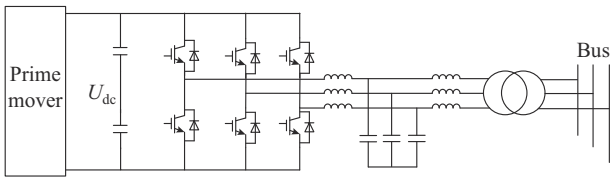

Fig. 9. Simplified model of IIDG utilized in hardware platform and PSCAD/EMTDC.

In order to evaluate the correctness of the proposed RMG protection strategy, an RMG shown in Fig. 2 is simulated in PSCAD/EMTDC. The root mean square value of the line voltage and the frequency of the system are 10 kV and 50 Hz, respectively. The grid-feeding IIDGs adopt the proposed current-based fault control strategy shown in Fig. 5. The capacities of grid-feeding IIDGs, grid-forming IIDG, and utility grid are 500 kVA, 2000 kVA, and 30 MVA, respectively [35], [36]. The maximum output fault currents of grid-feeding IIDGs and grid-forming IIDG are 2 and 5 times the rated current, respectively [2], [22]. The capacities of three-phase symmetrical loads LD1, LD2, and LD3 are (1200 + j30)kVA [35], [36]. The positive-sequence impedance of the feeders is (0.38 + j0.45)Ω/km, and the zero-sequence impedance is (0.76 + j1.32)Ω/km [37]. The length of feeders AB, BC, and AD is 2 km, and IIDGs and loads are connected to the bus through 0.1 km feeders.

A. Verification of Current-based Fault Control Strategy

A simplified power-electronics-based hardware platform with the controller TMS320F28335 is fabricated, as shown in Appendix A Fig. A1. This platform mainly comprises a grid-forming IIDG, a grid-feeding IIDG, and the loads. The hardware platform specifications are presented in Table I. During the normal operation, the condition that the voltage of the grid-forming IIDG suddenly drops is used to simulate the RMG fault condition. The experimental result is depicted in Fig. 10.

TABLE I
Hardware Platform Specifications

Parameter	Value
Nominal microgrid voltage	220 V
Nominal microgrid frequency	50 Hz
DC-link voltage	650 V
DC-link capacitance	1600 μF
AC filter capacitance	3.3 μF
Inductance	2.4 mH
Switching frequency	10 kHz
Delay time t (in e^{-st})	40 ms

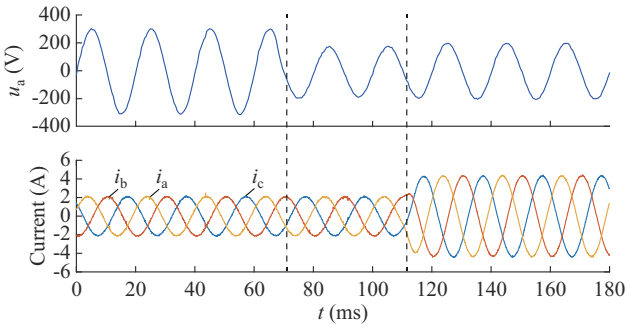

Fig. 10. Experimental result of hardware platform.

The grid-forming IIDG only outputs the positive-sequence voltage, thus its voltages are symmetrical and the phase-a voltage u_a is shown in Fig. 10. When u_a suddenly drops, the currents of the grid-feeding IIDG i_a, i_b, and i_c will remain the pre-fault output current for two cycles, as shown in Fig. 10. During this period, the specific fault characteristics will be generated. Afterwards, the grid-feeding IIDG adopts the LVRT control strategy. Owing to their rapidity of control and response, IIDGs can generate the specific fault characteristics in the specific time and transit to the LVRT mode rapidly. Thus, the effectiveness of the proposed current-based fault control strategy is verified.

Based on the PSCAD/EMTDC platform, in islanded mode, when $t=0.3$ s, a phase-phase fault occurs in the midpoint of feeder B2C1 and the transition resistance is 3 Ω. IIDGs adopt the current-based fault control strategy. The voltage waveforms of the grid-forming IIDG (DG1) is shown in Fig. 11 and the current waveforms of the grid-feeding IIDG (DG2) is shown in Fig. 12.

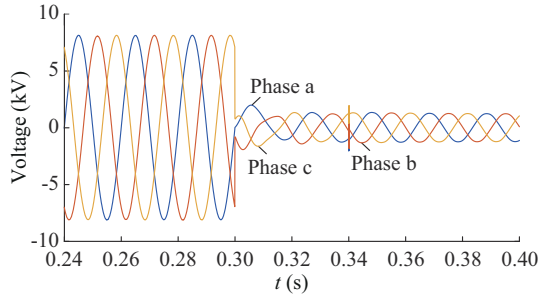

Fig. 11. Voltage waveforms of grid-forming IIDG (DG1).

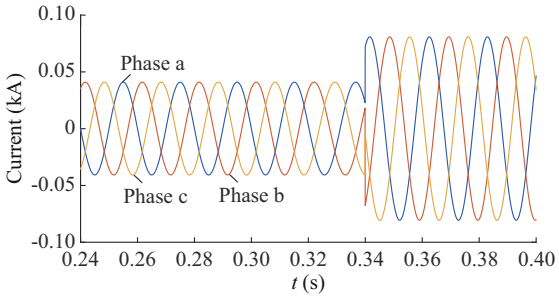

Fig. 12. Current waveforms of grid-feeding IIDG (DG2).

As can be seen from Fig. 12, the grid-feeding IIDGs can maintain the normal-running current for two cycles effectively and transit to LVRT mode smoothly. The simulation results in Fig. 11 and Fig. 12 are consistent with the experimental results in Fig. 10, which proves the effectiveness of the proposed current-based fault control strategy.

B. Verification of Proposed RMG Protection Strategy

The effectiveness of the proposed RMG protection strategy is verified in the following Cases 1-5. The RMG adopts ungrounded mode in Cases 1-4, thus the phase-phase and three-phase faults are verified. The grounded mode is adopted in Case 5, and a high-impedance single-phase-to-ground fault is verified.

Case 1: in grid-connected mode, when $t=0.3$ s, a three-phase fault occurs at the midpoint of feeder B2C1, and the transition resistance is 3 Ω. The amplitude, phase, and phase difference of pre-fault and during-fault positive-sequence voltages of each bus and those of PSCFCs on the feeders are shown in Tables II and III, respectively. The phase has been converted to the range of (–180°, 180°), and the phase difference represents the value of $|\varphi_{Ki}| = |\arg(\boldsymbol{u}_K) - \arg(\Delta\boldsymbol{i}_{Ki})|$. With the amplitudes and phase differences in Tables II and III, the fault directions of each feeder are determined.

As shown in the Tables II and III, the phase difference of A3 is 4.26°, so it is a forward feeder. The phase difference of B1 in the same feeder of A3 is 174.84°, thus it is a reverse fault feeder. It means that A3B1 is not the fault feeder. Both ends of B2C1 are forward fault feeders, which satisfies the fault detection criterion. Therefore, B2C1 is the fault feeder. For other main feeders such as A4D1, the fault detection criterion is not satisfied and they are detected as healthy feeders. For the branch feeders such as B4, C3, and D3, they are reverse fault feeders and are detected as healthy feeders. Therefore, the fault feeder B2C1 is located.

TABLE II
AMPLITUDE, PHASE, AND PHASE DIFFERENCE OF PRE-FAULT AND DURING-FAULT POSITIVE-SEQUENCE VOLTAGES OF EACH BUS IN CASE 1

Bus position	Electrical quantity	Amplitude (kV)	Phase (°)	Phase difference (°)
Bus A	$\boldsymbol{u}_{A,0}$	5.77	–0.08	
	$\boldsymbol{u}^{+}_{A,f}$	5.31	–3.41	
Bus B	$\boldsymbol{u}_{B,0}$	5.71	–0.82	
	$\boldsymbol{u}^{+}_{B,f}$	4.89	–7.43	
Bus C	$\boldsymbol{u}_{C,0}$	5.67	–1.12	
	$\boldsymbol{u}^{+}_{C,f}$	4.68	–9.71	
Bus D	$\boldsymbol{u}_{D,0}$	5.73	–0.43	
	$\boldsymbol{u}^{+}_{D,f}$	5.32	–3.44	

TABLE III
AMPLITUDE, PHASE, AND PHASE DIFFERENCE OF PSCFCS ON FEEDERS IN CASE 1

Bus position	Electrical quantity	Amplitude (A)	Phase (°)	Phase difference (°)
Bus A	$\Delta\boldsymbol{i}_{A1}$	2533.00	–4.36	4.28
	$\Delta\boldsymbol{i}_{A2}$	1.00		
	$\Delta\boldsymbol{i}_{A3}$	1793.00	–4.34	4.26
	$\Delta\boldsymbol{i}_{A4}$	2.00	–150.18	150.10
Bus B	$\Delta\boldsymbol{i}_{B1}$	2535.00	175.66	174.84
	$\Delta\boldsymbol{i}_{B2}$	1796.00	–4.27	3.45
	$\Delta\boldsymbol{i}_{B3}$	2.00		
	$\Delta\boldsymbol{i}_{B4}$	5.00	–136.02	135.20
Bus C	$\Delta\boldsymbol{i}_{C1}$	5.13	27.95	29.07
	$\Delta\boldsymbol{i}_{C2}$	0		
	$\Delta\boldsymbol{i}_{C3}$	6.43	–136.01	134.89
Bus D	$\Delta\boldsymbol{i}_{D1}$	2.00	29.47	29.90
	$\Delta\boldsymbol{i}_{D2}$	1.00		
	$\Delta\boldsymbol{i}_{D3}$	3.00	–136.02	135.59

Case 2: in grid-connected mode, when $t=0.3$ s, a phase-phase fault occurs in the midpoint of feeder B2C1 and the transition resistance is 3 Ω. The amplitude, phase, and phase difference of pre-fault and during-fault positive-sequence voltages of each bus and those of PSCFCs on the feeders in this case are shown in Tables IV and V, respectively.

Compared with the Case 1, the amplitude of PSCFCs decreases, and the amplitude of the positive-sequence voltage of each bus slightly increases after the fault. B2 and C1 are detected as forward fault feeders as well. Therefore, the fault feeder can be located accurately through the proposed fault detection criterion.

TABLE IV
AMPLITUDE, PHASE, AND PHASE DIFFERENCE OF PRE-FAULT AND DURING-FAULT POSITIVE-SEQUENCE VOLTAGES OF EACH BUS IN CASE 2

Bus position	Electrical quantity	Amplitude (kV)	Phase (°)	Phase difference (°)
Bus A	$\boldsymbol{u}_{A,0}$	5.77	–0.08	
	$\boldsymbol{u}^{+}_{A,f}$	5.60	–1.35	
Bus B	$\boldsymbol{u}_{B,0}$	5.71	–0.82	
	$\boldsymbol{u}^{+}_{B,f}$	5.44	–2.77	
Bus C	$\boldsymbol{u}_{C,0}$	5.67	–1.12	
	$\boldsymbol{u}^{+}_{C,f}$	5.35	–3.51	
Bus D	$\boldsymbol{u}_{D,0}$	5.73	–0.43	
	$\boldsymbol{u}^{+}_{D,f}$	5.60	–1.38	

TABLE V
AMPLITUDE, PHASE, AND PHASE DIFFERENCE OF PSCFCS ON FEEDERS IN CASE 2

Bus position	Electrical quantity	Amplitude (A)	Phase (°)	Phase difference (°)
Bus A	$\Delta\boldsymbol{i}_{A1}$	2366	–7.88	7.80
	$\Delta\boldsymbol{i}_{A2}$	1		
	$\Delta\boldsymbol{i}_{A3}$	1681	–7.87	7.79
	$\Delta\boldsymbol{i}_{A4}$	2	–152.93	152.85
Bus B	$\Delta\boldsymbol{i}_{B1}$	2377	172.12	172.94
	$\Delta\boldsymbol{i}_{B2}$	1684	7.80	8.62
	$\Delta\boldsymbol{i}_{B3}$	1		
	$\Delta\boldsymbol{i}_{B4}$	5	–139.50	138.68
Bus C	$\Delta\boldsymbol{i}_{C1}$	5	25.15	26.27
	$\Delta\boldsymbol{i}_{C2}$	0		
	$\Delta\boldsymbol{i}_{C3}$	6	–139.42	138.30
Bus D	$\Delta\boldsymbol{i}_{D1}$	2	26.72	27.15
	$\Delta\boldsymbol{i}_{D2}$	1		
	$\Delta\boldsymbol{i}_{D3}$	2	–139.53	139.10

Case 3: in islanded mode, when $t=0.3$ s, a three-phase fault occurs in the midpoint of B2C1 feeder and the transition resistance is 3 Ω. The amplitude, phase, and phase difference of pre-fault and during-fault positive-sequence voltages of each bus and those of PSCFCs on the feeders in this case are shown in Tables VI and VII, respectively.

TABLE VI
AMPLITUDE, PHASE, AND PHASE DIFFERENCE OF PRE-FAULT AND DURING-FAULT POSITIVE-SEQUENCE VOLTAGES OF EACH BUS IN CASE 3

Bus position	Electrical quantity	Amplitude (kV)	Phase (°)	Phase difference (°)
Bus A	$\boldsymbol{u}_{A,0}$	5.72	–0.11	
	$\boldsymbol{u}^{+}_{A,f}$	1.21	–19.11	
Bus B	$\boldsymbol{u}_{B,0}$	5.66	–0.73	
	$\boldsymbol{u}^{+}_{B,f}$	1.13	–21.43	
Bus C	$\boldsymbol{u}_{C,0}$	5.62	–1.09	
	$\boldsymbol{u}^{+}_{C,f}$	1.09	–22.70	
Bus D	$\boldsymbol{u}_{D,0}$	5.69	–0.51	
	$\boldsymbol{u}^{+}_{D,f}$	1.21	–19.01	

TABLE VII
AMPLITUDE, PHASE, AND PHASE DIFFERENCE OF PSCFCS ON FEEDERS IN CASE 3

Bus position	Electrical quantity	Amplitude (A)	Phase (°)	Phase difference (°)
Bus A	$\Delta\boldsymbol{i}_{A1}$	0		
	$\Delta\boldsymbol{i}_{A2}$	543	137.98	138.09
	$\Delta\boldsymbol{i}_{A3}$	584	–36.61	36.50
	$\Delta\boldsymbol{i}_{A}$	87	–179.47	179.36
Bus B	$\Delta\boldsymbol{i}_{B1}$	826	143.41	144.14
	$\Delta\boldsymbol{i}_{B2}$	630	–33.32	32.59
	$\Delta\boldsymbol{i}_{B3}$	0		
	$\Delta\boldsymbol{i}_{B}$	61	–178.84	178.11
Bus C	$\Delta\boldsymbol{i}_{C1}$	58	2.24	3.33
	$\Delta\boldsymbol{i}_{C2}$	0		
Bus D	$\Delta\boldsymbol{i}_{D1}$	54	–20.31	19.80
	$\Delta\boldsymbol{i}_{D2}$	0		
	$\Delta\boldsymbol{i}_{D3}$	60	–178.82	178.31

Compared with the Case 1, the RMG is disconnected to the utility grid. Since it lacks the fault current contribution of the utility grid, the amplitude of the positive-sequence voltage of each bus significantly decreases after the fault. It reflects that the fault severity of Case 3 is more serious than that of Case 1. But it does not affect the phase relationship between the PSCFCs and the pre-fault bus voltage. The fault feeder B2C1 can still be located accurately through the proposed fault detection criterion.

Case 4: in islanded mode, when $t=0.3$ s, a phase-phase fault occurs in the midpoint of B2C1 feeder and the transition resistance is 3 Ω. The amplitude, phase, and phase difference of pre-fault and during-fault positive-sequence voltages of each bus and those of PSCFCs on the feeders in this case are shown in Tables VIII and IX, respectively.

TABLE VIII
AMPLITUDE, PHASE, AND PHASE DIFFERENCE OF PRE-FAULT AND DURING-FAULT POSITIVE-SEQUENCE VOLTAGES OF EACH BUS IN CASE 4

Bus position	Electrical quantity	Amplitude (kV)	Phase (°)	Phase difference (°)
Bus A	$\boldsymbol{u}_{A,0}$	5.71	–0.11	
	$\boldsymbol{u}^{+}_{A,f}$	2.21	5.29	
Bus B	$\boldsymbol{u}_{B,0}$	5.66	–0.73	
	$\boldsymbol{u}^{+}_{B,f}$	2.18	5.20	
Bus C	$\boldsymbol{u}_{C,0}$	5.62	–1.09	
	$\boldsymbol{u}^{+}_{C,f}$	2.16	5.16	
Bus D	$\boldsymbol{u}_{D,0}$	5.69	–0.51	
	$\boldsymbol{u}^{+}_{D,f}$	2.21	5.28	

Compared with the Case 3, the amplitude of the PSCFCs is lower and the amplitude of the positive-sequence voltage of each bus is higher. It reflects that the fault severity of Case 4 is relatively lighter than that of Case 3. The fault feeder B2C1 can still be located accurately.

TABLE IX
AMPLITUDE, PHASE, AND PHASE DIFFERENCE OF PSCFCS ON FEEDERS IN CASE 4

Bus position	Electrical quantity	Amplitude (A)	Phase (°)	Phase difference (°)
Bus A	$\Delta \boldsymbol{i}_{A1}$	0		
	$\Delta \boldsymbol{i}_{A2}$	269	120.88	120.99
	$\Delta \boldsymbol{i}_{A3}$	296	–52.31	52.20
	$\Delta \boldsymbol{i}_{A4}$	43	175.72	175.83
Bus B	$\Delta \boldsymbol{i}_{B1}$	419	127.65	128.38
	$\Delta \boldsymbol{i}_{B2}$	327	–47.07	46.34
	$\Delta \boldsymbol{i}_{B3}$	1		
	$\Delta \boldsymbol{i}_{B4}$	47	175.11	176.57
Bus C	$\Delta \boldsymbol{i}_{C1}$	43	–4.01	2.92
	$\Delta \boldsymbol{i}_{C2}$	1		
	$\Delta \boldsymbol{i}_{C3}$	43	175.10	176.19
Bus D	$\Delta \boldsymbol{i}_{D1}$	43	–3.11	2.60
	$\Delta \boldsymbol{i}_{D2}$	0		
	$\Delta \boldsymbol{i}_{D3}$	43	174.98	175.49

Case 5: in islanded and grounded mode, when $t = 0.3$ s, a high-impedance single-phase-to-ground fault occurs in the midpoint of B2C1 feeder and the transition resistance is 100 Ω. The amplitude, phase, and phase difference of pre-fault and during-fault positive-sequence voltages of each bus and those of PSCFCs on the feeders in this case are shown in Tables X and XI, respectively.

TABLE X
AMPLITUDE, PHASE, AND PHASE DIFFERENCE OF PRE-FAULT AND DURING-FAULT POSITIVE-SEQUENCE VOLTAGES OF EACH BUS IN CASE 5

Bus position	Electrical quantity	Amplitude (kV)	Phase (°)	Phase difference (°)
Bus A	$\boldsymbol{u}_{A.0}$	5.72	–0.11	
	$\boldsymbol{u}^{+}_{A.f}$	5.72	–0.17	
Bus B	$\boldsymbol{u}_{B.0}$	5.66	–0.73	
	$\boldsymbol{u}^{+}_{B.f}$	5.66	–0.99	
Bus C	$\boldsymbol{u}_{C.0}$	5.63	–1.09	
	$\boldsymbol{u}^{+}_{C.f}$	5.62	–1.40	
Bus D	$\boldsymbol{u}_{D.0}$	5.69	–0.43	
	$\boldsymbol{u}^{+}_{D.f}$	5.69	–0.51	

As shown in the Table X, when a high-impedance fault occurs in RMG, the amplitude change of the positive-sequence voltage of each bus is not obvious. The PSCFC Δi_{B2} changes significantly and the fault feeder B2C1 can still be located accurately through the proposed fault detection criteria. Therefore, compared with the Cases 1-4, the proposed fault protection strategy is still valid for the grounded system under high-impedance fault.

Cases 1-5 present the simulation results of different grounded modes, fault types, and transition resistances. The negative-sequence components exist in Cases 1-4, while the zero-sequence components exist in Case 5.

TABLE XI
AMPLITUDE, PHASE, AND PHASE DIFFERENCE OF PSCFCS ON FEEDERS IN CASE 5

Bus position	Electrical quantity	Amplitude (A)	Phase (°)	Phase difference (°)
Bus A	$\Delta \boldsymbol{i}_{A1}$	0		
	$\Delta \boldsymbol{i}_{A2}$	9.43	173.29	173.40
	$\Delta \boldsymbol{i}_{A3}$	9.18	–6.64	6.53
	$\Delta \boldsymbol{i}_{A4}$	0.11	154.33	154.44
Bus B	$\Delta \boldsymbol{i}_{B1}$	13.00	176.34	177.07
	$\Delta \boldsymbol{i}_{B2}$	17.55	–5.55	4.82
	$\Delta \boldsymbol{i}_{B3}$	0		
	$\Delta \boldsymbol{i}_{B4}$	0.25	106.31	107.04
Bus C	$\Delta \boldsymbol{i}_{C1}$	0.31	43.83	44.92
	$\Delta \boldsymbol{i}_{C2}$	0		
	$\Delta \boldsymbol{i}_{C3}$	0.22	133.38	133.47
Bus D	$\Delta \boldsymbol{i}_{D1}$	0.16	156.57	157.00
	$\Delta \boldsymbol{i}_{D2}$	0		
	$\Delta \boldsymbol{i}_{D3}$	0.15	95.85	96.28

These two components only affect the fault starting criterion (8) but are independent of the proposed fault detection criteria (9) and (10).

Through the above simulation analysis, IIDGs using the current-based fault control strategy can generate specific fault characteristics when different types of faults occur in the RMG, which is consistent with the theoretical analysis in Section III. The RMG fault protection strategy proposed in Section IV can locate the fault feeder in both islanded and grid-connected RMGs accurately.

VI. DISCUSSION AND COMPARISON

This paper proposes an RMG fault protection strategy coordinating with a current-based fault control strategy. With the proposed current-based fault control strategy, IIDGs generate the specific fault characteristics and then adopt the LVRT strategy according to grid code.

By improving the protection scheme of the traditional distribution network, the effective protection techniques on microgrid are mainly sorted into five categories, which are overcurrent protection [10], voltage-based protection [11], differential protection [19], adaptive protection [14], and intelligent-algorithm-based protection [17]. As shown in Case 5, because the fault characteristics of current and voltage are not obvious, it is difficult for overcurrent protection and voltage-based protection to detect the high-impedance fault. The differential protection based on the communication network can be applied to any topology to detect all kinds of faults in theory. However, due to the small capacity and short feeders of microgrid, high communication speed is required, which will increase the cost. The adaptive protection is also based on the traditional communication network. It needs a CPU to process the data collected by phasor measurement units (PMUs), and then reset the threshold through intelligent algorithms. Compared with differential protection, adap-

tive protection requires more node data and better communication network. Intelligent-algorithm-based protection is usually combined with adaptive protection, which has strong robustness, good adaptive ability, and high steady control accuracy, so that it can flexibly cope with the structure and state changes of microgrid. However, like adaptive protection, intelligent-algorithm-based protection still needs a lot of PMUs and high-speed communication network. Compared with [14], [17], [19], owing to the delay in the control strategy, IIDGs can maintain specific fault characteristics for 2 cycles. Therefore, the proposed fault protection strategy does not need the high-speed communication network.

Although an RMG contains multiple types of RESs, they can all be equivalent to a voltage- or current-controlled source when different control strategies are applied. The main difficulty of RMG fault protection is the influence of IIDGs on fault characteristics. Most researches only focus on the identification of fault characteristics in RMGs but ignore the improvement of the fault control strategy of IIDGs. Although some researchers [30], [38] have begun to focus on this point, the proposed control strategies lack consideration for the coordination control of fault characteristics and voltage support. Compared with the existing fault detection and protection strategies, the superiorities of the proposed fault protection strategy are presented in Table XII, where √ and × represent the strategy with and without this scenario capability, respectively.

TABLE XII
SUPERIORITIES OF PROPOSED FAULT PROTECTION STRATEGY

Strategy	High-impedance fault	Low-speed communication	Fault control	Flexible LVRT	Coordination with control and protection
[10]	×	√	×	×	×
[11]	×	√	×	×	×
[19]	√	×	×	√	×
[14]	√	×	×	√	×
[17]	√	×	×	√	×
[30]	√	√	√	×	×
[35]	√	√	√	×	×
Proposed	√	√	√	√	√

The proposed fault protection strategy has the following advantages.

1) By adjusting the fault control strategy of IIDGs, the equivalent fault models of IIDGs can be changed, and the equivalent additional network of positive-sequence fault components can be simplified. In this way, without the complicated parameters or fault calculation, the fault feeder of every fault type in the RMG with different topologies and operation modes can be located.

2) With IIDGs adopting the current-based fault control strategy, the fault feeder can be accurately located during the delay cycle. Furthermore, IIDGs can track the LVRT reference after the delay cycle. Without modifying the control strategy of IIDGs complicatedly and adding expensive hardware protection devices, the fault component protection principle can still be applicable owing to the proposed fault control strategy. This fault control strategy takes both protection and voltage support of RMGs into account and realizes the coordination design of fault control of IIDGs and RMG protection strategy.

3) The calculation of PSCFCs only needs the pre-fault and during-fault current quantities. Therefore, the proposed current-based fault control strategy and fault detection criteria can be applicable in complex scenarios.

4) The proposed current-based fault control strategy is based on the low inertia, fast response, and high controllability characteristics of DGs, thus it can be widely utilized in PV, battery, type-4 WT generator, and other low-inertia IIDG systems.

5) Owing to the delay in the control strategy, IIDGs can maintain the specific fault characteristics for some periods. Therefore, the proposed fault detection criteria do not need high-speed communication network and are not affected by the performance of PLL.

VII. CONCLUSION

A current-based fault control strategy and a new RMG protection strategy based on fault component protection principle are proposed in this paper. Owing to the fault control strategy, specific fault characteristics are generated by IIDGs to ensure that the fault component protection principle is still applicable in the RMG, and based on this, the fault feeder can be located accurately. Then, IIDGs can transit to the LVRT mode smoothly. According to the analysis of fault characteristics, a new RMG fault detection criterion is proposed, which uses the phase difference between the PSCFC and the pre-fault bus voltage to locate the fault feeder. The proposed fault detection criteria are suitable for both grid-connected and islanded RMGs. The experimental and simulation results validate the correctness of the current-based fault control strategy and the effectiveness of the RMG fault protection strategy.

APPENDIX A

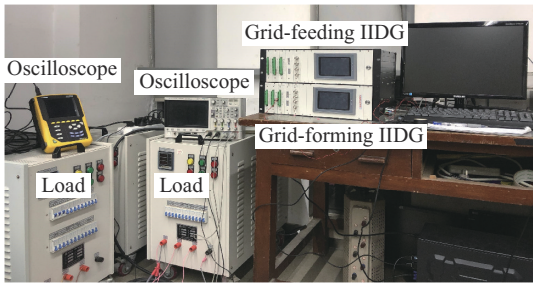

Fig. A1. Simplified power-electronics-based hardware platform.

REFERENCES

[1] A. A. Camilo, O. H. Sebastian, and W. David, "Single-dwelling and community renewable microgrids: optimal sizing and energy management for new business models," *Applied Energy*, vol. 254, pp. 1-17, Nov. 2019.

[2] Z. Liang, L. Mu, and F. Zhang, "The fault detection method of islanded microgrid with the V/f controlled distributed generation," *International Journal of Electrical Power & Energy Systems*, vol. 112, pp. 28-

35, Apr. 2019.
[3] B. Zhou, J. Zou, Y. Chi *et al*., "Multi-microgrid energy management systems: architecture, communication, and scheduling strategies," *Journal of Modern Power Systems and Clean Energy*, vol. 9, no. 3, pp. 463-476, May 2021.
[4] B. Patnaik, M. Mishra, R. C. Bansal *et al*., "MODWT-XGBoost based smart energy solution for fault detection and classification in a smart microgrid," *Applied Energy*, vol. 285, p. 116457, Mar. 2021.
[5] J. O. C. P. Pinto and M. Moreto, "Protection strategy for fault detection in inverter-dominated low voltage AC microgrid," *Electric Power Systems Research*, vol. 190, p. 106572, Jan. 2021.
[6] P. T. Manditereza and R. C. Bansal, "Protection of microgrids using voltage-based power differential and sensitivity analysis," *International Journal of Electrical Power & Energy Systems*, vol. 18, p. 105756, Jan. 2020.
[7] D. E. Olivares, A. Mehrizi-Sani, A. H. Etemadi *et al*., "Trends in microgrid control," *IEEE Transactions on Smart Grid*, vol. 5, no. 4, pp. 1905-1919, Jul. 2014.
[8] F. Zhang and L. Mu, "A fault detection method of microgrid with grid-connected inverter interfaced distributed generators based on the PQ control strategy," *IEEE Transactions on Smart Grid*, vol. 10, no. 5, pp. 4816-4826, Sept. 2019.
[9] H. Bahramian-Habil, H. A. Abyaneh, and G. B. Gharehpetian, "Improving LVRT capability of microgrid by using bridge-type fault current limiter," *Electric Power Systems Research*, vol. 191, p. 106872, Feb. 2021.
[10] E. C. Piesciorovsky and N. N. Schulz, "Comparison of non-real-time and real-time simulators with relays in-the-loop for adaptive overcurrent protection," *Electric Power Systems Research*, vol. 143, pp. 657-668, Feb. 2016.
[11] H. Al-Nasseri, M. A. Redfern, and F. Li, "A voltage based protection for micro-grids containing power electronic converters," in *Proceedings of IEEE PES General Meeting*, Montreal, Canada, Oct. 2006, pp. 1-7.
[12] V. A. F. Almeida, G. N. Taranto, and J. M. T. Marinho, "Phasor-domain dynamic model of asymmetric current injection controller for converter-interfaced generator," *Journal of Modern Power Systems and Clean Energy*, vol. 9, no. 6, pp. 1269-1278, Nov. 2021.
[13] S. M. Saad, N. El-Naily, and F. A. Mohamed, "A new constraint considering maximum PSM of industrial over-current relays to enhance the performance of the optimization techniques for microgrid protection schemes," *Sustainable Cities and Society*, vol. 44, pp. 445-457, Jan. 2019.
[14] M. S. Elbana, N. Abbasy, A. Meghed *et al*., "μPMU-based smart adaptive protection scheme for microgrids," *Journal of Modern Power Systems and Clean Energy*, vol. 7, no. 3, pp. 887-898, May 2019.
[15] L. Strezoski, I. Stefani, and D. Bekut, "Novel method for adaptive relay protection in distribution systems with electronically-coupled DERs," *International Journal of Electrical Power & Energy Systems*, vol. 116, pp. 22-31, Mar. 2020.
[16] H. Li, C. Deng, Z. Zhang *et al*., "An adaptive fault-component-based current differential protection scheme for distribution networks with inverter-based distributed generators," *International Journal of Electrical Power & Energy Systems*, vol. 128, p. 106719, Jun. 2021.
[17] A. Yilmaz and G. Bayrak, "A real-time UWT-based intelligent fault detection method for PV-based microgrids," *Electric Power Systems Research*, vol. 177, pp. 190-202, Dec. 2019.
[18] M. Majidi and M. Etezadi-Amoli, "A new fault location technique in smart distribution networks using synchronized/nonsynchronized measurements," *IEEE Transactions on Power Delivery*, vol. 33, no. 3, pp. 1358-1368, Jun. 2018.
[19] T. S. Aghdam, H. K. Karegar, and H. H. Zeineldin, "Variable tripping time differential protection for microgrids considering DG stability," *IEEE Transactions on Smart Grid*, vol. 10, no. 3, pp. 2407-2415, May 2019.
[20] A. Soleimanisardoo, H. K. Karegar, and H. H. Zeineldin, "Differential frequency protection scheme based on off-nominal frequency injections for inverter-based islanded RMGs," *IEEE Transactions on Smart Grid*, vol. 10, no. 2, pp. 2107-2114, Mar. 2019.
[21] C. D. Prasad, M. Biswal, and A. Y. Abdelaziz, "Adaptive differential protection scheme for wind farm integrated power network," *Electric Power Systems Research*, vol. 187, p. 106452, Oct. 2020.
[22] B. Wang and L. Jing. "A protection method for inverter-based microgrid using current-only polarity comparison," *Journal of Modern Power Systems and Clean Energy*, vol. 8, no. 3, pp. 446-453, May 2020.
[23] I. Sadeghkhani, M. E. H. Golshan, A. Mehrizi-Sani *et al*., "Transient monitoring function-based fault detection for inverter-interfaced microgrids," *IEEE Transactions on Smart Grid*, vol. 9, no. 3, pp. 2097-2107, May 2018.
[24] A. Cagnano, E. de Tuglie, and P. Mancarella, "Microgrids: overview and guidelines for practical implementations and operation," *Applied Energy*, vol. 258, no. 15, p. 114039, Jan. 2020.
[25] S. Admasie, S. B. A. Bukhari, T. Gush *et al*., "Intelligent islanding detection of multi-distributed generation using artificial neural network based on intrinsic mode function feature," *Journal of Modern Power Systems and Clean Energy*, vol. 8, no. 3, pp. 511-520, May 2020.
[26] W. C. Clarke, M. J. Brear, and C. Manzie, "Control of an isolated microgrid using hierarchical economic model predictive control," *Applied Energy*, vol. 280, no. 15, p. 115960, Dec. 2020.
[27] M. Beus, F. Banis, H. Pandžić *et al*., "Three-level hierarchical microgrid control – model development and laboratory implementation," *Electric Power Systems Research*, vol. 189, p. 106758, Dec. 2020.
[28] B. Liu, Z. Liu, J. Liu *et al*., "An adaptive virtual impedance control scheme based on small-AC-signal injection for unbalanced and harmonic power sharing in islanded microgrids," *IEEE Transactions on Power Electronics*, vol. 34, no. 12, pp. 12333-12355, Dec. 2019.
[29] M. Nadour, A. Essadki, and T. Nasser, "Improving low-voltage ride-through capability of a multimegawatt DFIG based wind turbine under grid faults," *Protection and Control of Modern Power Systems*, vol. 5, no. 4, pp. 370-382, Dec. 2020.
[30] Z. Chen, X. Pei, M. Yang *et al*., "A novel protection scheme for inverter-interfaced microgrid (IIM) operated in islanded mode," *IEEE Transactions on Industrial Electronics*, vol. 33, no. 9, pp. 7684-7697, Sept. 2018.
[31] K. O. Oureilidis and C. S. Demoulias, "A fault clearing method in converter-dominated microgrids with conventional protection means," *IEEE Transactions on Power Electronics*, vol. 31, no. 6, pp. 4628-4640, Jun. 2016.
[32] A. Hooshyar and R. Iravani, "A new directional element for microgrid protection," *IEEE Transactions on Smart Grid*, vol. 9, no. 6, pp. 6862-6876, Nov. 2018.
[33] H. Gao and P. A. Crossley, "Design and evaluation of a directional algorithm for transmission-line protection based on positive sequence fault components," *IEE Proceedings: Generation, Transmission & Distribution*, vol. 153, no. 6, pp. 711-718, Nov. 2006.
[34] L. Ji, X. Tao, Y. Fu *et al*., "A new single ended fault location method for transmission line based on positive sequence superimposed network during auto-reclosing," *IEEE Transactions on Power Delivery*, vol. 34, no. 3, pp. 1019-1029, Jun. 2019.
[35] A. Soleimanisardoo, H. K. Karegar, and H. H. Zeineldin, "Differential frequency protection scheme based on off-nominal frequency injections for inverter-based islanded microgrids," *IEEE Transactions on Smart Grid*, vol. 10, no. 2, pp. 2107-2114, Mar. 2019.
[36] A. H. K. Alaboudy, H. H. Zeineldin, and J. Kirtley, "Microgrid stability characterization subsequent to fault-triggered islanding incidents," *IEEE Transactions on Power Delivery*, vol. 27, no. 2, pp. 658-669, Apr. 2012.
[37] B. Mahamedi and J. E. Fletcher, "Trends in the protection of inverter-based microgrids," *IET Generation, Transmission & Distribution*, vol. 13, no. 2, pp. 4511-4522, Oct. 2019.
[38] M. A. Azzouz and A. Hooshyar, "Dual current control of inverter-interfaced renewable energy sources for precise phase selection," *IEEE Transactions on Smart Grid*, vol. 10, no. 5, pp. 5092-5102, Sept. 2019.

Zihao Wang received the M.S. degree from Guangxi University, Nanning, China, in 2018. He is currently pursuing the Ph.D. degree with Tongji University, Shanghai, China. His current research interests include microgrid protection and control.

Longhua Mu received the B.E., M.E., and Ph.D. degrees in electrical engineering from the China University of Mining and Technology, Xuzhou, China, in 1986, 1988, and 1998, respectively. He has been a Full Professor with the Department of Electrical Engineering, Tongji University, Shanghai, China, since 2004. His current research interests include power system protection and control, microgrid, integrated energy systems, and power electronics and its applications in power systems.

Chongkai Fang received the B. S. degree in electrical engineering from Tongji University, Shanghai, China, in 2020, where he is currently pursuing the Ph.D. degree. His current research interests include control and protection of microgrid and smart distribution network.